

# Predicting trends in atmospheric CO<sub>2</sub> across the Mid-Pleistocene Transition using existing climate archives

Jordan R.W. Martin<sup>1</sup>, Joel Pedro<sup>2,3</sup>, Tessa R. Vance<sup>3</sup>

<sup>1</sup>Institute for Marine and Antarctic Studies, University of Tasmania, Hobart, 7004, Australia

<sup>2</sup>Australian Antarctic Division, Kingston, 7050, Australia

<sup>3</sup>Australian Antarctic Program Partnership, Institute for Marine and Antarctic Studies, University of Tasmania, Hobart, 7004, Australia

*Correspondence to:* Jordan R.W. Martin (jrmartin@utas.edu.au)

## Abstract

During the Mid-Pleistocene Transition (MPT), ca. 1200–800 thousand years ago (kya), the Earth's glacial cycles changed from 41 kyr to 100 kyr periodicity. The emergence of this longer ice-age periodicity was accompanied by higher global ice volume in glacial periods and lower global ice volume in interglacial periods. Since there is no known change in external orbital forcing across the MPT, it is generally agreed that the cause of this transition is internal to the earth system. Resolving the climate, carbon cycle and cryosphere processes responsible for the MPT remains a major challenge in earth and palaeoclimate science. To address this challenge, the international ice core community has prioritised recovery of an ice core record spanning the MPT interval.

Here we present results from a simple generalised least squares (GLS) model that predicts atmospheric CO<sub>2</sub> out to 1.8 Myr. Our prediction utilises existing records of atmospheric carbon dioxide (CO<sub>2</sub>) from Antarctic ice cores spanning the past 800 kyr along with the existing LR04 benthic  $\delta^{18}\text{O}_{\text{calcite}}$  stack (Lisiecki & Raymo, 2005; hereafter 'benthic  $\delta^{18}\text{O}$  stack') from marine sediment cores. Our predictions assume that the relationship between CO<sub>2</sub> and benthic  $\delta^{18}\text{O}$  over the past 800 thousand years can be extended over the last one and a half million years. The implicit null hypothesis is that there has been no fundamental change in feedbacks between atmospheric CO<sub>2</sub> and the climate parameters represented by benthic  $\delta^{18}\text{O}$ , global ice volume and ocean temperature.

We test the GLS-model predicted CO<sub>2</sub> concentrations against observed blue ice CO<sub>2</sub> concentrations,  $\delta^{11}\text{B}$ -based CO<sub>2</sub> reconstructions from marine sediment cores and  $\delta^{13}\text{C}$  of leaf-wax based CO<sub>2</sub> reconstructions (Higgins *et al.*, Yan *et al.*, 2019 and Yamamoto *et al.*, 2022). We show that there is not clear evidence from the existing blue ice or proxy CO<sub>2</sub> data to reject our predictions nor our associated null-hypothesis. A definitive test and/or rejection of the null hypothesis may be provided following recovery and analysis of continuous oldest ice core records from Antarctica, which are still several years away. The record presented here should provide a useful comparison for the oldest ice core records and opportunity to provide further constraints on the processes involved in the MPT.

## 37 **1 Introduction**

38 Ice core records from Antarctica provide comprehensive and continuous records of many climate parameters  
39 over the last 800 thousand years, e.g. from the Vostok (Petit *et al.*, 1999) and European Project for Ice Coring in  
40 Antarctica's Dome-C (EDC) ice cores (Jouzel *et al.*, 2007). One of the major challenges in climate science lies  
41 beyond the current threshold of the ice core record. The Mid-Pleistocene Transition (MPT) spans from ca.  
42 1200–800 thousand years ago (kya) (Chalk *et al.*, 2017) and is characterised by a change from regularly paced  
43 40 thousand year (kyr) glacial cycles with thinner glacial ice sheets to quasi-periodic 100 kyr glacial cycles in  
44 which ice sheets are more persistent and thicker (Clark *et al.*, 2006, Chalk *et al.*, 2017). To resolve the forcings  
45 and feedbacks involved in this transition, multiple nations are targeting recovery of continuous ice cores  
46 spanning the MPT under the framework of the International Partnerships in Ice Core Science (IPICS) oldest ice  
47 core challenge (IPICS, 2020).

48

49 The purpose of the current study is to make a simple prediction of atmospheric CO<sub>2</sub> across the MPT. Cross-  
50 comparison of our and other predicted CO<sub>2</sub> records against observed MPT CO<sub>2</sub> data will aid in testing  
51 competing hypotheses on the cause of the transition, in particular the role of carbon cycle changes.

52

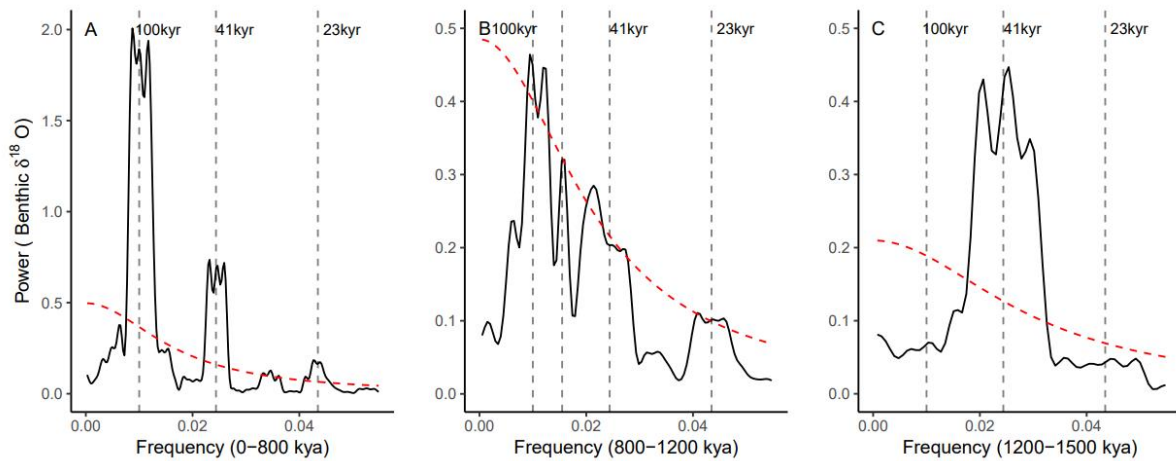
53 The MPT occurred in the absence of any changes to orbital insolation forcing; therefore, the mechanisms behind  
54 the MPT must be internal to the earth system (Raymo, 1997; Ruddiman *et al.*, 1989). Multiple hypotheses have  
55 been put forward to explain the transition. A common element in many of these is internal climate/earth system  
56 changes which allow for the development of thicker, more extensive ice sheets that could endure insolation  
57 peaks corresponding to the 23 kyr precession and 41 kyr obliquity cycles, i.e., an increase in the threshold for  
58 deglaciation and altered sensitivity to orbital forcings (McClymont *et al.*, 2013; Tzedakis *et al.*, 2017). Indeed,  
59 the skipped obliquity cycle hypothesis, proposes that 100 kyr signal seen in spectral analysis of the post-MPT  
60 benthic  $\delta^{18}\text{O}$  stack (e.g. Fig 1A) may be comprised of alternating 80 and 120-kyr signals, i.e. in which the  
61 intervening obliquity cycles are skipped. Among the prominent hypotheses to explain an increased threshold for  
62 deglaciation are the following three.

63 1) A long- term decrease in radiative forcing due to a secular reduction in atmospheric CO<sub>2</sub> across the  
64 transition (e.g. Berger *et al.*, Hönisch *et al.*, 2009; 1999, Raymo *et al.*, 1988). According to this view,  
65 reduced radiative forcing drives the formation of larger and more stable ice sheets.

66 2) Progressive removal of sub-glacial regolith during the 41 kyr glacial cycles. Clark & Pollard (1998)  
67 proposed that ice sheet basal sliding prior to the MPT was enhanced by the presence of a low-friction  
68 sedimentary regolith layer between the Laurentide ice sheet and the crystalline bedrock. According to  
69 this view, progressive removal of this sedimentary layer then favoured the development of larger and  
70 more persistent post-MPT ice sheets.

71 3) Phase-locking of the Northern and Southern Hemisphere ice sheets. In frequency spectra of the global  
72 marine benthic  $\delta^{18}\text{O}$  record (Fig. 1) there is no evidence of the precession (23 kyr) component of  
73 northern hemisphere insolation prior to the MPT; the spectra is dominated by the obliquity (41 kyr)  
74 component (Fig. 1C). Emergence of significant precession and 100 kyr signals occurs across the MPT  
75 (Fig. 1B), and all three components are clearly present after the MPT (Fig. 1A). Raymo *et al.* (2006)  
76 suggested that precession-paced changes in northern and southern hemisphere ice volumes may have

77 occurred prior to the MPT, but are cancelled due to out-of-phase ice volume changes between the two  
 78 hemispheres. According to this view, during the MPT the precession-paced changes fall into phase  
 79 between the two hemispheres, such that the precession signal emerges (Raymo *et al.*, 2006). In this  
 80 view the global synchronisation of ice volume drives the formation of larger and more stable ice sheets.  
 81  
 82 These hypotheses are not mutually exclusive. For a recent review on the cause of the MPT see Berends *et al.*  
 83 (2021a).  
 84



85  
 86  
 87 **Figure 1: Thomson Multi-taper Method (MTM) spectral analysis representing relative power of signal periodicity for:**  
 88 **A) Benthic  $\delta^{18}\text{O}$  stack after (0–800 kya) the Mid-Pleistocene Transition (MPT); B) Benthic  $\delta^{18}\text{O}$  across the MPT (800–**  
 89 **1200 kya); C) Benthic  $\delta^{18}\text{O}$  prior to the onset of the MPT (1200 kya–1500 kya). Each with a robust AR (1) 95 %**  
 90 **Confidence interval (red dashed line). Benthic  $\delta^{18}\text{O}$  stack data from Lisiecki and Raymo (2005).**  
 91

92 For a long-term decrease in radiative forcing by atmospheric  $\text{CO}_2$  to be the cause of the MPT, the reduction in  
 93  $\text{CO}_2$  might be expected in both glacial and interglacial stages (Chalk *et al.*, 2017). However, low resolution  
 94 boron-isotope-based  $\text{CO}_2$  reconstructions by Hönisch *et al.*, (2009), and Chalk *et al.*, (2017) suggest that glacial-  
 95 stage  $\text{CO}_2$  drawdown occurred over the MPT in the absence of interglacial  $\text{CO}_2$  drawdown. Glacial-stage  $\text{CO}_2$   
 96 draw-down across the MPT may be a positive climate-carbon cycle feedback to changes in ice sheet dynamics,  
 97 including  $\text{CO}_2$  drawdown by enhanced iron fertilisation of the Southern Ocean in response to exposed  
 98 continental shelves due to lower sea level, as well as planetary drying associated with colder climate conditions  
 99 (Chalk *et al.*, 2017). Colder glacial temperatures that enhance the solubility of  $\text{CO}_2$  in the oceans, and reduced  
 100 abyssal ocean ventilation has also been implicated in enhanced glacial-stage ocean storage of  $\text{CO}_2$  (McClymont  
 101 *et al.*, 2013; Hasenfratz *et al.*, 2019).  
 102

103 Testing of hypotheses on the cause of the MPT is currently limited by the lack of a continuous ice core that  
 104 spans its duration. The International Partnership in Ice Core Sciences (IPICS) has nominated recovery of such a  
 105 record as a key priority in ice core research (IPICS, 2020). Multiple national and international projects have  
 106 commenced, or are soon to commence, drilling for ‘oldest ice’ (see e.g. Shugi, 2022). In this project, we take  
 107 inspiration from the “EPICA Challenge” in which the paleoclimate and modeling community was challenged to

108 predict the global atmospheric carbon dioxide and methane concentrations from 800–400 kya based on the  
109 existing 400 kyr Vostok ice core record (Wolff *et al.*, 2004). Here, we use a generalised least squares (GLS)  
110 model trained on continuous climate archives to predict a CO<sub>2</sub> record out 1.8 Mya. We utilise two primary data  
111 sets for the GLS model: the existing 800 kyr ice core composite record of atmospheric CO<sub>2</sub> (Bereiter *et al.*,  
112 2015) and the LR04 benthic stack of 57 globally-distributed records of the <sup>18</sup>O to <sup>16</sup>O ratio of fossil benthic  
113 foraminifera calcite (hereafter referred to as the LR04  $\delta^{18}\text{O}$  benthic stack). The  $\delta^{18}\text{O}$  ratios in the LR04 benthic  
114 stack are governed primarily by deep ocean temperature and global ice volume at the time the foraminifera  
115 lived, with higher values indicating both increased ice volume and a colder climate. The relationship between  
116 the ice volume and ocean temperature components contributing to the  $\delta^{18}\text{O}$  benthic stack are not linear.  
117 Separating the two signals remains challenging and has been attempted elsewhere using a range of approaches  
118 from comparison with paired deep ocean temperature proxies (Elderfield *et al.*, 2012), inverse modelling  
119 (Berends *et al.*, 2021b) and spectral analysis (e.g. Huybers and Wunsch, 2009).

120

121 Fig. 2 shows a scatter-plot of the LR04  $\delta^{18}\text{O}$  benthic stack versus observed ice core CO<sub>2</sub> over the past 800 kyr.  
122 Both data sets are binned to equivalent 3-kyr time steps (Methods). The Pearson's correlation coefficient (*r*)  
123 between the data sets is -0.82 (*p* < 0.05) indicating that ~68% of the variance in observed CO<sub>2</sub> is shared with the  
124 LR04  $\delta^{18}\text{O}$  benthic stack. This strong relationship provides an initial rationale for using the LR04  $\delta^{18}\text{O}$  benthic  
125 stack as an input parameter to predict CO<sub>2</sub> beyond 800 kyr. Mechanistically, multiple processes are expected to  
126 contribute to the shared variance. A first order factor is the dependency of CO<sub>2</sub> solubility on ocean temperature  
127 (e.g. Millero, 1995). From the simple solubility perspective, colder climate states with increased ice volume and  
128 colder ocean temperatures will drive increased ocean uptake of CO<sub>2</sub> (Berends *et al.*, 2021a). However, the  
129 solubility effect only accounts for a portion of observed glacial CO<sub>2</sub> drawdown (Archer *et al.*, 2000). Multiple  
130 additional contributors to the shared variance are proposed in the literature. These include (not exhaustively),  
131 direct radiative forcing of ice volume changes by CO<sub>2</sub> (e.g. Shackleton *et al.*, 1985); the impact of ice  
132 volume/sea level changes on atmospheric CO<sub>2</sub> via ocean productivity and carbonate chemistry changes (e.g.  
133 Broecker, 1982; Archer *et al.*, 2000; Ushie and Matsumoto, 2012); CO<sub>2</sub> drawdown during periods of high ice  
134 volume by increased iron fertilisation (e.g. Röthlisberger *et al.*, 2004; Martinez-Garcia *et al.*, 2014) and  
135 enhanced sea ice extent during periods of high ice volume capping the ventilation of CO<sub>2</sub> from the ocean  
136 interior at high latitudes (Stephens and Keeling, 2000).

137

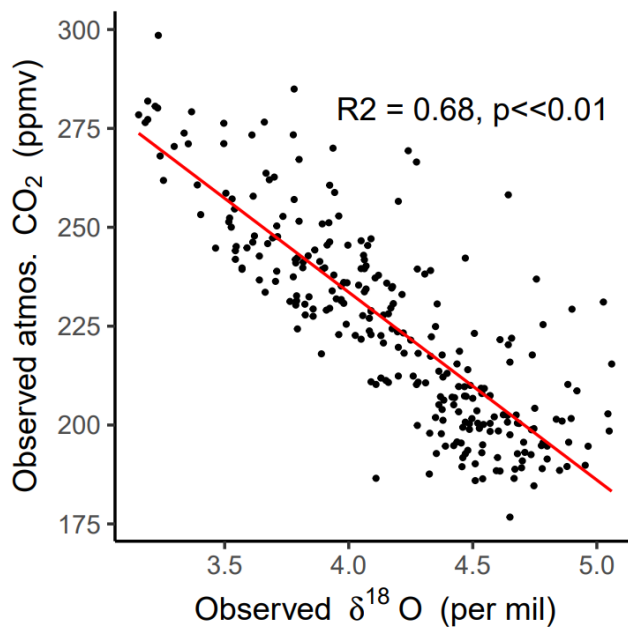
138 A quantitative separation and attribution of the processes linking global ice volume, ocean temperature and  
139 atmospheric CO<sub>2</sub> on millennial to orbital timescales is not currently available (e.g. Archer *et al.*, 2000; Sigman  
140 *et al.*, 2010; Gottschalk *et al.*, 2019) and will not be attempted here. Rather, we make the simple assumption that  
141 the relationships between the LR04 benthic  $\delta^{18}\text{O}$  stack and CO<sub>2</sub> can be extended beyond 800 kya and use  
142 generalised least squares (GLS) regression modelling between benthic  $\delta^{18}\text{O}$  and CO<sub>2</sub> to make a prediction of  
143 CO<sub>2</sub> spanning 800–1500 kya. The deliberately simple implicit assumption, and null hypothesis, is that there is  
144 no change to the feedback processes linking benthic  $\delta^{18}\text{O}$  and CO<sub>2</sub> before and after the MPT.

145

146 This approach differs to previous more complex model studies that have attempted to reconstruct CO<sub>2</sub> using the  
147 LR04 benthic  $\delta^{18}\text{O}$  stack as an input variable (van de Wal, 2011; Stap *et al.*, 2016, Berends *et al.*, 2021b). The

148 latter studies use an inverse forward modelling approach, in which climate and ice sheet models of various  
 149 complexities are used to capture physical relations between CO<sub>2</sub>, global temperature and ice volume. For  
 150 example, in Berends *et al.*, 2021b the offset between modelled and observed benthic δ<sup>18</sup>O is used to calculate a  
 151 value for atmospheric CO<sub>2</sub> that is iterated back to the inverse model. The CO<sub>2</sub> record which minimises the  
 152 difference between the modelled and observed benthic stack is then taken as an estimate of how atmospheric  
 153 CO<sub>2</sub> may have evolved to force coupled climate, deep ocean temperature and land ice volume changes that  
 154 reproduce the observed benthic δ<sup>18</sup>O signal. Accuracy of the reconstructions in the inverse modelling approach  
 155 depends on the ability of the climate and ice sheet models used to capture the correct climate dynamics across  
 156 the MPT. Our GLS method is a simpler statistical approach, designed with the specific null hypothesis in mind,  
 157 that does not attempt to simulate the physics linking benthic δ<sup>18</sup>O signal, land ice volume, global temperature  
 158 and CO<sub>2</sub>. A range of approaches to reconstructing CO<sub>2</sub> have been called for and are of value in the context of  
 159 forthcoming continuous ice core records across the MPT from oldest ice projects currently underway in  
 160 Antarctica [IPICS 2020].

161



162 **Figure 2: Scatter plot of the composite observed atmospheric CO<sub>2</sub> record (Bereiter *et al.*, 2015) against**  
 163 **the LR04 benthic stack of marine δ<sup>18</sup>O records (Lisiecki & Raymo, 2005). Red line is a linear line of best**  
 164 **fit ( $R^2 = 0.68$ ;  $p < 0.05$ ).**

165

166 To test our null hypothesis, in advance of the recovery of a continuous ice core, we compare our predicted CO<sub>2</sub>  
 167 record to two sets of low-resolution ice core data that exist outside the current 800 kyr observed CO<sub>2</sub>. These data  
 168 come from direct CO<sub>2</sub> measurements from ancient “blue ice” from the Allan Hills in East Antarctica (hereafter  
 169 referred to as BI-CO<sub>2</sub>) from ca. 1 Mya (Higgins *et al.*, 2015) and 1.5 Mya (Yan *et al.*, 2022). We use the term  
 170 blue ice to describe deep, ancient glacial ice that has been brought nearer to the surface of an ice sheet by ice  
 171 flow. Blue ice is sampled by cutting trenches or shallow drilling of up to several hundred meters (e.g. Higgins *et*  
 172 *al.*, 2015). The vertical migration of blue ice is associated with high deformation making the ice samples  
 173 stratigraphically complex and hard to date (Higgins *et al.*, 2015). As a result, blue ice records alone do not

174 provide a continuous CO<sub>2</sub> record across the MPT. In the Discussion, we also compare our predicted record to  
175 existing proxy-CO<sub>2</sub> reconstructions from boron-isotope analysis of benthic foraminifera in marine sediment  
176 records (Chalk, *et al.*, 2017; Dyez *et al.*, 2018; Guillermic *et al.*, 2022), leaf wax δ<sup>13</sup>C carbon isotope ratios  
177 (Yamamoto *et al.*, 2022) and predictions from previous models of various complexities (van de Wal *et al.*, 2011;  
178 Willeit *et al.* 2019; Berends *et al.* 2021b). We conclude with discussion of the implications of our results and  
179 data-comparisons for the understanding MPT dynamics.

180

## 181 **2 Methods**

182

183 We use a generalised least squares (GLS) model with an auto-regressive (AR) factor 1 to predict atmospheric CO<sub>2</sub>  
184 from the LR04 benthic δ<sup>18</sup>O stack (Fig. 3A and B). We use GLS because the assumptions of ordinary least squares  
185 (OLS) are violated by the presence of autocorrelation and heteroskedasticity in the regression errors. We selected  
186 the AR(1) correlation factor as it yielded the lowest Akaike information criterion (AIC) value from a test of  
187 multiple correlation factors. The AR(1) process assumes and accounts for dependence of error at a given point in  
188 time on the previous error term. In practise this makes the model assumptions more realistic and improves  
189 parameter estimation where, as in the climate system, observations are dependent on past values.

190

191 To obtain common time steps and resolution between the predictor (LR04 benthic δ<sup>18</sup>O stack) and response  
192 (CO<sub>2</sub>) variables, we re-grid the LR04 benthic stack and Bereiter *et al.*, (2015) CO<sub>2</sub> data into time bins with a  
193 resolution of 3-kyr. The GLS regression model was then applied over the 0 – 800 kyr range of the predictor and  
194 response variables as follows:

195

$$196 \quad CO_2 = -33.37 \times \delta^{18}O + 365.15, \text{ autoregressive (AR) factor: } 1$$

197

198 Based on the regression model, the δ<sup>18</sup>O values of the LR04 Benthic Stack from 800 – 1500 kya were used to  
199 predict CO<sub>2</sub> concentration over this range (hereafter referred to as PRED-CO<sub>2</sub>). To gauge the GLS model  
200 stability we took a bootstrap approach, selecting a random 50% subset of our data (with replacement) and re-  
201 running the model 1000 times to determine 95% confidence intervals for the predictions. While the GLS method  
202 itself addresses autocorrelation, the bootstrap method introduces variability such that each iteration of the model  
203 has different combinations of the original data points (including repeated ones), this variability helps in  
204 assessing the robustness and sensitivity of the model e.g. to variable data and dating uncertainty.

205

206 Uncertainties in the independent age scales of both the LR04 stack and the compiled CO<sub>2</sub> record are inherited by  
207 our GLS model and its predictions. The LR04 stack includes 57 globally-distributed benthic δ<sup>18</sup>O sediment core  
208 records. The age models for these cores are constructed by alignment of their δ<sup>18</sup>O signals, followed by tuning  
209 of the stack to a simple ice model based on 21 June insolation at 65°N in a way which maintains relatively  
210 stable global mean sedimentation rates. (Lisiecki & Raymo, 2005). The authors estimate uncertainty of 6 kyr  
211 from 1.5 – 1.0 Mya and 4 kyr from 1 – 0 Mya (Lisiecki & Raymo, 2005). The observed CO<sub>2</sub> composite ice core  
212 record for the past 800 kya (Bereiter *et al.*, 2015) uses six independent dating methods for various core locations  
213 both spatially across Antarctica, and stratigraphically for different sections of the same core. The age uncertainty  
214 in the gas timescale has a median over the 0 – 800 kya interval of 2 kyr, but individual uncertainties can reach

215 up to 5 kyr (Veres *et al* 2013; Bazin *et al.*, 2013). The relative age uncertainties between these input variables  
216 may diminish the regression or in some instances lead to spurious correlation. However, we expect any such  
217 effects are minor on the basis that our predictions show little sensitivity to the bootstrap analysis; with a median  
218  $2\sigma$  error of 5.8 ppm from 0 to 1.8 Mya (see Fig. 3B, C and Discussion).

219

### 220 **3 Results**

221 Fig. 3B shows the time series of our LR04 benthic  $\delta^{18}\text{O}$  stack-based GLS model predictions of atmospheric  $\text{CO}_2$   
222 (PRED- $\text{CO}_2$ ) over the past 800 kyr, in comparison to the observed ice core  $\text{CO}_2$  record from Bereiter *et al.*,  
223 (2015). The correlation coefficient ( $R^2$ ) between the predicted and observed records is 0.68 ( $p \ll 0.01$ ). Our  
224 PRED- $\text{CO}_2$  record out to 1.8 Mya with shaded 95% CIs from the bootstrap analysis is also shown, overlain with  
225 observed Allan Hills blue ice  $\text{CO}_2$  (BI- $\text{CO}_2$ ) datasets of age  $1000 \pm 89$  kya (Higgins *et al.*, 2015) and  $1.5 \text{ Mya} \pm$   
226  $213$  kyr (Yan *et al.*, 2022).

227

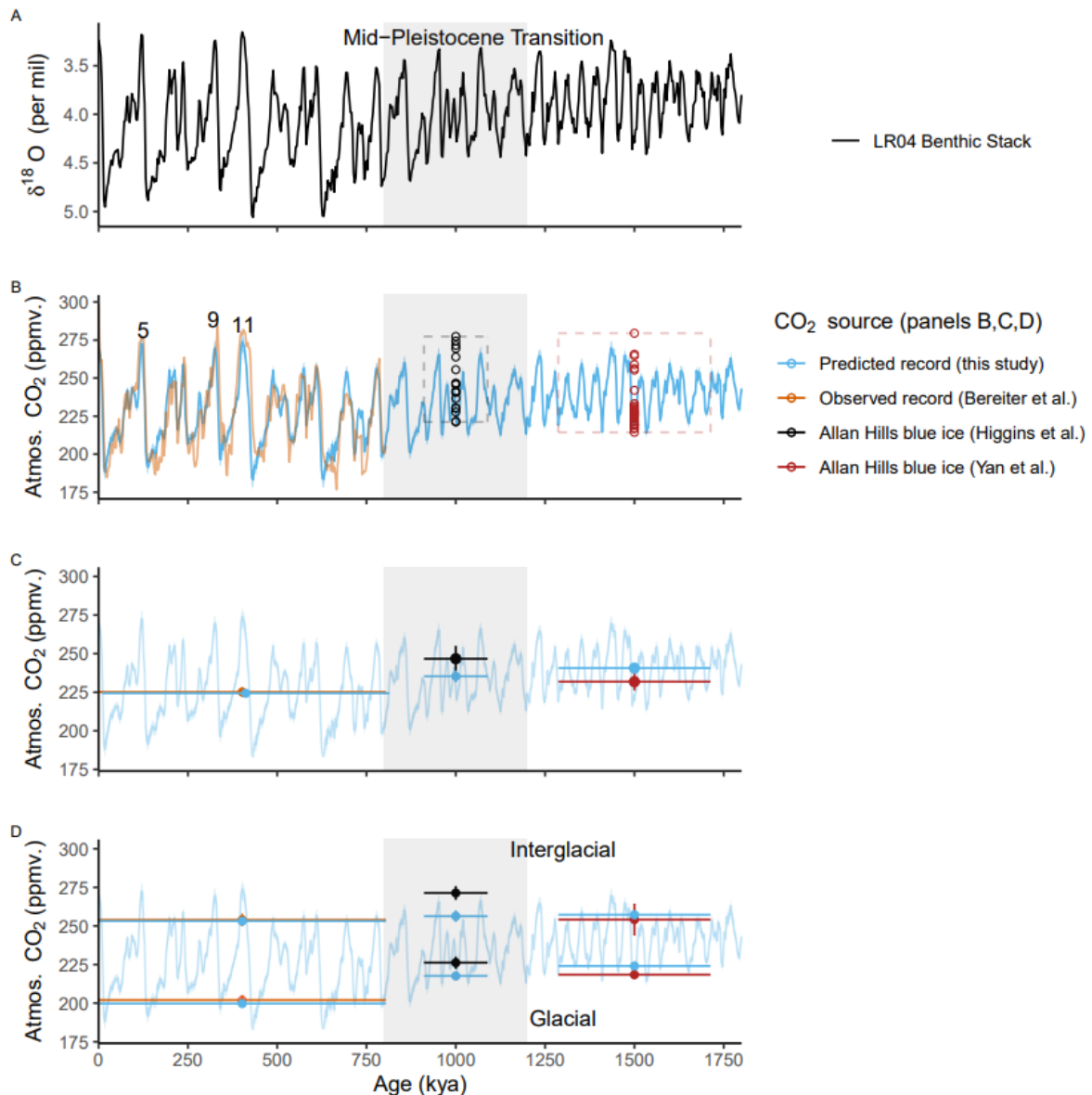
228 We evaluate the PRED- $\text{CO}_2$  record against the observed  $\text{CO}_2$  data according to criteria of mean concentrations  
229 across the common intervals, and mean concentrations in the glacial and interglacial subsets of the data. First,  
230 the mean  $\text{CO}_2$  concentration over the common intervals (Fig 3C). From 0 – 800 kya the mean concentration in  
231 observed (Bereiter *et al.*, 2015) and PRED- $\text{CO}_2$  data are in close agreement ( $225.2 \pm 3.03$  ppm versus the  
232 predicted  $225.2 \pm 2.5$  ppm respectively; uncertainties are 95% confidence intervals, i.e.  $1.96\sigma$ ). In the  $1000 \pm 89$   
233 kya interval (i.e. averaged across the age uncertainty of the Higgins *et al.* (2015) blue ice data) the BI- $\text{CO}_2$   
234 concentration is  $\sim 11$  ppm higher than PRED- $\text{CO}_2$  ( $246.7 \pm 8.4$  ppm versus the predicted  $235.3 \pm 3.9$  ppm), this  
235 difference is not significant at the 95% confidence level. For the  $1.5 \text{ Mya} \pm 213$  kyr interval, the mean BI- $\text{CO}_2$   
236 concentration is  $\sim 9$  ppm lower than PRED- $\text{CO}_2$  ( $231.9 \pm 5.6$  ppm versus the predicted  $240.7 \pm 2.1$  ppm), which  
237 is marginally significant at the 95% level. Comparisons of mean levels across intervals spanning multiple glacial  
238 and interglacial cycles may be biased if (as is likely) the blue ice data is not sampling glacial and interglacial  
239 values with the same uniformity as a continuous record.

240

241 To address this, we define the glacial and interglacial thresholds of PRED- $\text{CO}_2$  to be respectively the lower and  
242 upper 25<sup>th</sup> percentiles of the LR04  $\delta^{18}\text{O}$  predictor variable (following Chalk *et al.*, 2017). Filtering the observed  
243 (Bereiter *et al.*, 2015)  $\text{CO}_2$  record and our predicted  $\text{CO}_2$  record according to these definitions we find a very  
244 close match for glacial ( $202.0 \pm 3.2$  versus the predicted  $199.7 \pm 1.6$  ppm) and interglacial intervals ( $253.9 \pm 4.1$   
245 ppm versus the predicted  $253.1 \pm 2.3$  ppm), over the past 800 kya (see Fig. 3D for these comparisons). For blue  
246 ice (BI- $\text{CO}_2$ ) data, a corresponding LR04 isotope signal could not be confidently applied to the measured  $\text{CO}_2$   
247 concentration due to the uncertainties associated with blue ice dating; therefore, we defined the glacial and  
248 interglacial thresholds of blue ice data according to the top (interglacial) and bottom (glacial) 25<sup>th</sup> percentiles of  
249 actual  $\text{CO}_2$ . Applying this to the  $1000 \pm 89$  kya interval finds that observed BI- $\text{CO}_2$  data is  $\sim 9$  ppm higher than  
250 PRED- $\text{CO}_2$  during the glacial stages ( $226.2 \pm 4.0$  ppm versus the predicted  $217.6 \pm 2.3$  ppm) and  $\sim 15$  ppm  
251 higher than PRED- $\text{CO}_2$  during the interglacial stages ( $271.3 \pm 4.5$  versus the predicted  $256.3 \pm 3.8$  ppm). These  
252 differences are significant with respect to the constrained uncertainties. During the  $1.5 \text{ Mya} \pm 213$  kyr interval,  
253 the mean BI- $\text{CO}_2$  concentration did not show any significant difference to PRED- $\text{CO}_2$  in interglacial stages  
254 ( $254.1 \pm 10.3$  versus the predicted  $257.2 \pm 1.7$  ppm. During glacial stages there is a small 2.9 ppm difference

255 between the upper estimate of BI-CO<sub>2</sub> and the lower estimate of PRED-CO<sub>2</sub> ( $218.4 \pm 1.3$  and  $224 \pm 1.4$  ppm  
 256 respectively, see Fig 3D). In our view these results, notwithstanding the 2.9 ppm difference at 1.5 Mya, do not  
 257 give sufficient cause to reject the GLS model. Furthermore, the comparison indicates that PRED-CO<sub>2</sub> is not  
 258 drifting systematically away from the existing observed BI-CO<sub>2</sub> data (Fig 3D). The differences could of course  
 259 be a failing in the model, potential biases in the blue ice data, dating uncertainty and/or other unconstrained  
 260 uncertainties (see Discussion for blue ice caveats).

261



262  
 263 **Figure 3: A) The LR04 Benthic Stack of 57 globally distributed δ<sup>18</sup>O records (Lisiecki & Raymo, 2005).**  
 264 **B) Comparison of our PRED-CO<sub>2</sub> (ppm) record to the current continuous composite record (0–800 kya);**  
 265 **and to direct CO<sub>2</sub> measurements from Allan Hills blue ice cores (BI-CO<sub>2</sub>) ca. 1 Mya ( $\pm 89$  kyr) (Higgins *et***  
 266 ***al.*, 2015) and ca. 1.5 Mya ( $\pm 213$  kyr) (Yan *et al.*, 2022). Age uncertainty boundaries for the BI-CO<sub>2</sub> data**  
 267 **are represented by dashed box boundaries. Marine isotope stages 5, 9, and 11 are numbered on the plot**  
 268 **according to Lisiecki & Raymo (2005). Blue shading around PRED-CO<sub>2</sub> is the 95% CI from bootstrap**  
 269 **analysis. C) Mean concentrations of the PRED-CO<sub>2</sub> and observed composite CO<sub>2</sub> records over the range**



270 **of the observed composite record (offset for clarity), and the mean concentrations of the PRED-CO<sub>2</sub> and**  
271 **BI-CO<sub>2</sub> data at 1 Mya and again at 1.5 Mya averaged over the age uncertainty range of each BI-CO<sub>2</sub> data**  
272 **set. D) As for C) however filtered by the upper and lower 25<sup>th</sup> and 75<sup>th</sup> percentiles to estimate glacial and**  
273 **interglacial periods.**

274

275 We now consider long-term trends in interglacial and (separately) glacial CO<sub>2</sub> levels across the past 1.8 Myr in  
276 PRED-CO<sub>2</sub> and in the existing ice core CO<sub>2</sub> data. For PRED-CO<sub>2</sub> there is no significant difference between CO<sub>2</sub>  
277 concentrations in the interglacial stages of the 1.5 Mya ± 213 kya, 1000 ± 89 kya and 0–800 kya windows (Fig 4  
278 D, blue bars). In the ice core observations, interglacial levels at 1.5 Mya in BI-CO<sub>2</sub> are also within the  
279 uncertainties of those in the 0–800 kya interval. Notably, the BI-CO<sub>2</sub> concentrations in the 1000 ± 89 kya  
280 interval appear elevated with respect to the 0–800 kyr and 1.5 Mya ± 213 kya intervals, however this elevated  
281 (ca. 271 ppm) level is consistent with the observed interglacial CO<sub>2</sub> concentration during interglacials 5, 9 and  
282 11 (Fig 3B). Overall, there is no indication in the observed ice core CO<sub>2</sub> data or in PRED-CO<sub>2</sub> for a long-term  
283 trend in *interglacial* CO<sub>2</sub> levels across the past 1.8 Myr.

284

285 In comparison, there are significant declines in glacial CO<sub>2</sub> levels across the MPT in PRED-CO<sub>2</sub> and the  
286 observed ice core data. For PRED-CO<sub>2</sub>, glacial CO<sub>2</sub> concentrations are not significantly different during the 1.5  
287 Mya ± 213 kya and 1000 ± 89 kya windows. However, across the MPT, PRED-CO<sub>2</sub> glacial concentrations drop  
288 by ~18 ppm (Fig 3D). This pattern is similar to the observed BI-CO<sub>2</sub> data, where glacial CO<sub>2</sub> levels show no  
289 decline between the 1.5 Mya ± 213 kya and 1000 ± 89 kya windows (indeed there is a marginal increase from  
290 218.4 ± 1.3 to 226.2 ± 4.0 ppm, respectively), before falling by 24 ppm to the 0–800 kyr observed glacial mean  
291 of 202.0 ± 3.2 ppm (Fig 3D). Glacial-stage draw-down of CO<sub>2</sub> across the MPT in the absence of interglacial  
292 draw-down is consistent with previous observations based on the boron-isotope-based CO<sub>2</sub> reconstructions (e.g.,  
293 Chalk *et al.*, 2017; Hönlisch *et al.*, 2009 and see Discussion). In the following section we also compare PRED-  
294 CO<sub>2</sub> data to boron-isotope-based and other CO<sub>2</sub> proxy records covering the 0 to 1.8 Myr interval.

295

#### 296 **4 Discussion**

297 Our objective with this manuscript was to generate the simplest reasonable model to predict CO<sub>2</sub> from the LR04  
298 δ<sup>18</sup>O benthic stack and to test the predictions against available observations. It is possible that the fit between  
299 observed and our predicted CO<sub>2</sub> data could be further improved using a non-linear approach. However, we  
300 refrain from a non-linear approach for several key reasons. First, a scatter plot of the LR04 δ<sup>18</sup>O benthic stack  
301 versus observed ice core CO<sub>2</sub> over the past 800 kyr yields a Pearson's correlation coefficient (R) of -0.82 (Fig.  
302 2), indicating that ~68% of the variance in observed CO<sub>2</sub> is shared with the benthic stack. This is similar to that  
303 reported in ordinary linear least-squares regression (R<sup>2</sup>=0.70) by Berends *et al.* (2021b). Importantly, there is no  
304 evidence in this scatter plot for departure from the linear relationship at high or low CO<sub>2</sub> or benthic δ<sup>18</sup>O levels.  
305 Second, following the approach of Chalk *et al.*, 2017 and interpreting the upper 25<sup>th</sup> percentile of CO<sub>2</sub> data as  
306 representing mean interglacial stage CO<sub>2</sub> and the lower 25<sup>th</sup> percentile of CO<sub>2</sub> data as representing mean glacial  
307 stages CO<sub>2</sub> levels, we see that our predicted interglacial mean value for the past 800 kyr (253.1 ± 2.3 ppm)  
308 closely overlaps with the observed interglacial mean value (253.9 ± 4.1 ppm) and similarly, the predicted glacial  
309 stage mean (199.7 ± 1.7 ppm) closely overlaps with the observed glacial stage mean (202.0 ± 3.2 ppm). Third,

310 the predictions are remarkably insensitive to bootstrap analysis in which 50 % of that data are omitted with each  
311 iteration of the GLS model. Such insensitivity to the bootstrap analysis and accurate prediction of glacial and  
312 interglacial state CO<sub>2</sub> values would be unlikely in the case of major non-linear dependencies between the LR04  
313 predictor and CO<sub>2</sub> response variables. Fourth, non-linear approaches would risk generating an improved fit due  
314 to statistical artefacts that do not meaningfully relate to any dependence between benthic δ<sup>18</sup>O and CO<sub>2</sub>. Finally,  
315 the specific causes and sources and sinks involved in glacial to interglacial and millennial-scale CO<sub>2</sub> variations  
316 remain poorly constrained (e.g. Archer *et al.*, 2000; Sigman *et al.*, 2010; Gottschalk *et al.*, 2019). Given this  
317 process-uncertainty, the GLS model fits our criteria of the simplest reasonable model. Further, the use of benthic  
318 δ<sup>18</sup>O to predict atmospheric CO<sub>2</sub> has precedence; in response to the EPICA challenge (Wolff *et al.*, 2004) N.  
319 Shackleton predicted atmospheric CO<sub>2</sub> out to 800 kyr, based on a number of benthic δ<sup>18</sup>O records from the East  
320 Pacific (Wolff, 2005).

321

322 There are several caveats with blue ice data that may affect its use to evaluate our GLS model predictions. The  
323 blue ice data may have been subject to diffusional smoothing of CO<sub>2</sub> (e.g. Yan *et al.*, 2019), which would act in  
324 the direction of elevating the (lower 25<sup>th</sup> percentile) assumed glacial concentrations above the glacial  
325 atmospheric values and reducing the (upper 25<sup>th</sup> percentile) assumed interglacial concentrations. There is also  
326 the potential for artificially elevated CO<sub>2</sub> concentrations in blue ice due in-situ respiration of CO<sub>2</sub> due to  
327 microbial activity in detrital matter. Respiration effects are screened for by measurements of δ<sup>13</sup>C of CO<sub>2</sub>,  
328 however it is difficult to demonstrate that all samples are unaffected (Yan *et al.*, 2019). These uncertainties  
329 support our argument that the GLS-model predictions are not rejected by the available observed BI-CO<sub>2</sub> data.

330

331 We consider the BI-CO<sub>2</sub> data to provide the most reliable measurements of CO<sub>2</sub> concentration, in the absence of  
332 a continuous ice core record across the MPT. However, further comparison of our CO<sub>2</sub> predictions can also be  
333 made against CO<sub>2</sub> proxy data from non-ice core archives (Fig 4A). We consider here δ<sup>11</sup>B-based atmospheric  
334 CO<sub>2</sub> reconstructions (Chalk *et al.*, 2017, Dyez *et al.* 2018 and Guillermic *et al.* 2022) and a recent atmospheric  
335 CO<sub>2</sub> reconstruction from δ<sup>13</sup>C of leaf wax (Yamamoto *et al.*, 2022). The continuous δ<sup>11</sup>B-based reconstructions  
336 of Dyez *et al.*, (2018) overlap PRED-CO<sub>2</sub> from ~1.38 – 1.5 Mya while the Chalk *et al.*, (2017) reconstruction  
337 overlaps PRED-CO<sub>2</sub> from 1.09 – 1.43 Mya. Discrete reconstructions from Guillermic *et al.* (2022) are  
338 distributed non-uniformly across the ~800 to 1.5 Mya interval. For the two continuous δ<sup>11</sup>B-based  
339 reconstructions (Chalk *et al.*, (2017) and Dyez *et al.*, (2018)) the glacial CO<sub>2</sub> levels appear consistent with the  
340 PRED-CO<sub>2</sub> record, within their reported 30 – 60 ppm uncertainties. However, δ<sup>11</sup>B-based interglacial stages in  
341 these reconstructions exceed those of the PRED-CO<sub>2</sub> record (Fig. 4A). The Guillermic *et al.* (2022)  
342 reconstructions suggest a larger range of CO<sub>2</sub> concentrations than the overlapping intervals of PRED-CO<sub>2</sub> and of  
343 the two continuous δ<sup>11</sup>B-based reconstructions (Fig. 4A). The large range of the Guillermic *et al.* (2022) data  
344 and the high interglacial maxima in the Chalk *et al.* (2017) and Dyez *et al.*, (2018) data, all significantly exceed  
345 the range and interglacial maxima from the BI-CO<sub>2</sub> estimates. These discrepancies internally between different  
346 δ<sup>11</sup>B-based CO<sub>2</sub> reconstructions and between the δ<sup>11</sup>B-based reconstructions and the BI-CO<sub>2</sub> data, may be due to  
347 uncertainties associated with the δ<sup>11</sup>B proxy transfer function. The δ<sup>11</sup>B-based CO<sub>2</sub> reconstructions are  
348 dependent on assumptions about multiple components of the carbonate system, including local marine carbon  
349 chemistry and the CO<sub>2</sub> saturation state in the past (Hönisch *et al.*, 2009). Evidence that δ<sup>11</sup>B-based

350 reconstructions may overestimate interglacial stage CO<sub>2</sub> is also seen in data from Chalk *et al.*, (2017) spanning  
351 ca. 0–250 kya, where the δ<sup>11</sup>B-based interglacial CO<sub>2</sub> levels exceed the continuous ice core CO<sub>2</sub> record by up to  
352 ca. 30 ppm.

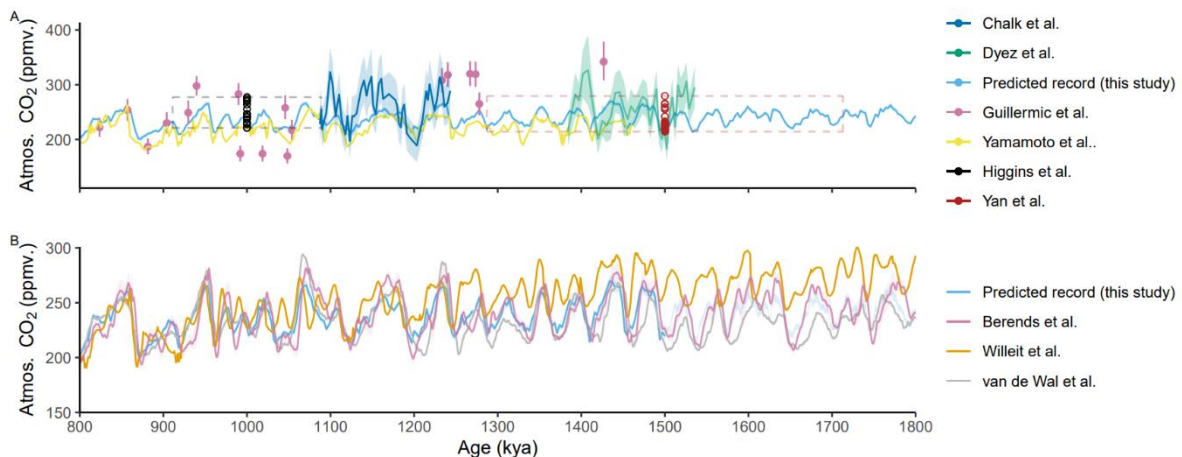
353

354 By comparison, the δ<sup>13</sup>C of leaf wax data (Yamamoto *et al.*, 2022) has a similar glacial to interglacial range as  
355 PRED-CO<sub>2</sub>, but a ca. 20ppm lower mean concentration than our predictions (Fig 4A). Hence, our PRED-CO<sub>2</sub>  
356 data fall lower than interglacial δ<sup>11</sup>B-based interglacial levels but are higher than the δ<sup>13</sup>C of leaf-wax based  
357 estimate. The strong spread between these different proxies and the large associated uncertainty of the  
358 alternative marine and leaf wax proxy-CO<sub>2</sub> reconstructions mean that we do not find cause from the existing  
359 CO<sub>2</sub> proxy data to reject our predictions nor our associated null-hypothesis.

360

361 We also compare our predictions to existing more complex model simulations (Fig 4B.). First, against a  
362 transient simulation using an intermediate-complexity earth system model (CLIMBER-2) by Willeit *et al.*  
363 (2019). This study suggests a combination of gradual regolith removal and atmospheric CO<sub>2</sub> decline can explain  
364 the long-term climate variability over the past 3 Myr. Second, against a longer-term reconstruction by van de  
365 Wal *et al.* (2011), which uses benthic δ<sup>18</sup>O that utilises deep-sea benthic isotope records to reconstruct a  
366 continuous CO<sub>2</sub> record over the past 20 Myr. Third, a CO<sub>2</sub> reconstruction based on an inverse forward-  
367 modelling approach forced by the LR04 benthic stack, in which the forward model is incrementally updated  
368 through interaction with general circulation model snapshots and the ANICE 3-D ice-sheet-shelf model  
369 (Berends *et al.* 2021b). Our simple GLS model demonstrates a similar long-term trend and timing of glacial-  
370 interglacial signals and an atmospheric CO<sub>2</sub> level that sits approximately mid-way between the van de Wal *et al.*  
371 (2011), and Willeit *et al.* (2019) models and is remarkably similar to the Berends *et al.* (2021b) reconstruction,  
372 despite their different approach. Notably the Berends *et al.* reconstruction shows greater glacial to interglacial  
373 amplitude in the CO<sub>2</sub> signal compared to our GLS-model. The decreasing linear trend in CO<sub>2</sub> in Willeit *et al.*  
374 (2019), which is not seen in the other reconstructions, was directly prescribed in that study to induce Northern  
375 Hemisphere glaciation at 2.6 Myr ago.

376



377

378 **Figure 4: A) Predicted CO<sub>2</sub> (this work) compared to observed, proxy CO<sub>2</sub> estimates from a range of other**  
379 **sources: δ<sup>11</sup>B-based pCO<sub>2</sub> reconstructions and measurements by Dyez *et al.* (2018), Guillermic *et al.***  
380 **(2022); Chalk *et al.*, (2017); blue ice CO<sub>2</sub> measurements by Yan *et al.* (2019) and Higgins *et al.* (2015);**

381  **$\delta^{13}\text{C}$  leaf wax proxy reconstructions by Yamamoto *et al.* (2022). The dashed boxes indicate the dating**  
382 **uncertainty and range of the respective BI-CO<sub>2</sub> records. B) Our predicted record compared to various**  
383 **model simulations: a regolith removal hypothesis simulation by Willeit *et al.* (2019); and inverse-model**  
384 **based CO<sub>2</sub> reconstructions by van de Wal *et al.* (2011), and Berends *et al.*, (2021b).**

385

386 A complete and critical test of our and other CO<sub>2</sub> predictions awaits the upcoming analysis of the continuous  
387 oldest ice core records. We now discuss some potential applications of the PRED-CO<sub>2</sub> record for hypothesis  
388 testing on the cause of the MPT.

389

390 PRED-CO<sub>2</sub> shows a long-term decline in glacial CO<sub>2</sub> across the MPT, but no long-term decrease in interglacial  
391 CO<sub>2</sub>. This pattern is consistent with the boron-isotope-based CO<sub>2</sub> reconstructions shown earlier, where it is often  
392 described as an increase in the interglacial to glacial CO<sub>2</sub> difference (e.g., Chalk *et al.*, 2017; Hönisch *et al.*,  
393 2009). Chalk *et al.*, (2017) concludes that the MPT was initiated by a change in ice sheet dynamics and that  
394 longer and higher-ice volume post-MPT ice ages are sustained by carbon cycle feedbacks, in particular dust  
395 fertilisation of the Southern Ocean. The fact that our LR04-based prediction of CO<sub>2</sub> captures this same trend,  
396 with predicted glacial CO<sub>2</sub> fairly constant from 1.5 to ca. 1.0 Mya before declining from 1.0 to 0.6 Mya, reflects  
397 that the LR04 benthic stack also features an increase in the interglacial to glacial benthic  $\delta^{18}\text{O}$  difference across  
398 this same interval, which is dominated by the glacial stage changes (Fig 3A.). Here, a comparison of PRED-CO<sub>2</sub>  
399 to a realised continuous oldest ice core record will be of value. The agreement or disagreement would inform on  
400 the proportionality of the CO<sub>2</sub> coupling with ice volume; if there were a major new or non-linear process across  
401 the MPT that changed the nature of coupling between CO<sub>2</sub> and ice volume the PRED-CO<sub>2</sub> and observed CO<sub>2</sub>  
402 records would be expected to diverge.

403

404 Another avenue to use the PRED-CO<sub>2</sub> record for hypothesis testing on the cause of the MPT concerns the phase  
405 locking hypothesis. The phase locking hypothesis is proposed to explain the absence of precession-related (23  
406 kyr) periods in the LR04 benthic stack prior to the MPT (Fig 1), despite the strong precession cycle in insolation  
407 (Raymo *et al.*, 2006, Morée *et al.*, 2021). The key concept is that prior to the MPT the Northern Hemisphere and  
408 Antarctic ice sheets were responsive (in ice volume) to insolation changes in the precession band, but because  
409 precession forcing is out of phase between the hemispheres, the ice volume changes were opposing between the  
410 hemispheres and therefore cancelled in the benthic stack. This cancellation of the precession signal left  
411 insolation forcing in the 41 kyr obliquity band to dominate globally integrated ice volume changes expressed in  
412 the benthic stack. A transition from a smaller and more dynamic terrestrial-terminating Antarctic ice sheet to a  
413 larger and more stable marine-terminating ice sheet with cooling climate across the MPT (e.g. Elderfield *et al.*,  
414 2012) is then proposed to remove sensitivity of Antarctic ice volume to local precession forcing in favour of  
415 quasi-100 kyr ice volume changes that are in phase between the hemispheres (Raymo *et al.*, 2006).

416

417 Recently presented data from Yan *et al.* (2022), lend some support to the phase locking hypothesis, specifically  
418 with evidence that pre-MPT Antarctic temperature (and by extension ice volume) is positively correlated with a  
419 local precession-band insolation proxy based on the oxygen to nitrogen ratio of trapped air (Yan *et al.*, 2022).  
420 Whereas the correlation becomes negative in the blue ice and continuous ice core data in the post-MPT record.

421 If Yan *et al.*, (2022) is correct and the phase locking hypothesis holds, then an implication is that prior to the  
422 MPT, Antarctic climate, Antarctic ice volume and by extension Southern Ocean climate conditions, would fall  
423 out of phase with the LR04 benthic stack. To now extend the argument to potential impacts on CO<sub>2</sub> exchange, if  
424 the phase locking hypothesis holds, then prior to the MPT the Antarctic and Southern Ocean climate conditions  
425 and by extension the Southern Ocean mechanisms of CO<sub>2</sub> exchange described earlier, would also be expected to  
426 fall out of phase with the benthic stack. Since our regression model assumes continuation of the in-phase  
427 relationship between the benthic stack and Antarctic and Southern Ocean climate conditions (as inherited from  
428 the post-MPT training data) we would expect to see major disagreement between our pre-MPT CO<sub>2</sub> predictions  
429 and a realised oldest ice continuous ice core CO<sub>2</sub> record.

430

## 431 **5 Summary and Conclusions**

432 In this study we have used a simple generalised least squares (GLS) model to predict atmospheric CO<sub>2</sub> from the  
433 LR04 benthic  $\delta^{18}\text{O}$  stack for the period spanning the mid-Pleistocene transition, 800–1800 kyr. Our CO<sub>2</sub>  
434 prediction is therefore based on the assumption that the physical processes linking CO<sub>2</sub>, sea level, global ice  
435 volume and ocean temperature over the past 800 kyr do not fundamentally change across the 800–1800 kya time  
436 period. The null-hypothesis is deliberately simplistic on the basis that differences between our predictions and  
437 observed or proxy CO<sub>2</sub> records may be revealing of the physical processes involved in the mid-Pleistocene  
438 Transition.

439

440 We made initial tests of the null hypothesis by comparing our predicted CO<sub>2</sub> record to existing discrete blue ice  
441 CO<sub>2</sub> records and other non-ice-core proxy-CO<sub>2</sub> records from the 800–1800 kyr interval. Our predicted CO<sub>2</sub>  
442 concentrations do not show any systematic departure from observed blue ice CO<sub>2</sub> concentrations. The  
443 predictions are marginally lower (during glacial *and* interglacial stages) than those observed in blue ice from  
444  $1000 \pm 89$  kya and marginally higher than observed in blue ice data from  $1.5 \text{ Mya} \pm 213$  kyr. Our predictions  
445 were generally lower than interglacial  $\delta^{11}\text{B}$ -based-CO<sub>2</sub> reconstructions, but higher than recent  $\delta^{13}\text{C}$  of leaf-wax  
446 based CO<sub>2</sub> reconstructions. Overall, we do not find clear evidence from the existing blue ice or proxy CO<sub>2</sub> data  
447 to reject our predictions nor our associated null-hypothesis. The definitive test of our and other CO<sub>2</sub> predictions  
448 therefore awaits the future analysis of the upcoming continuous oldest ice core records. The PRED-CO<sub>2</sub> record  
449 presented here should provide a useful comparison to forthcoming oldest ice core records and opportunity to  
450 provide further constraints on the processes involved in the MPT.

451

## 452 **Author contributions**

453 Project design by JBP, TRV and JRWM and supervision by TRV and JBP. Data analysis and figures by JRWM  
454 with input from all authors. Writing led by JRMV and JBP. All authors contributed to and agreed on the final  
455 version of the manuscript.

456

## 457 **Competing interests**

458 The authors declare that they have no competing interests.

459

460 **Disclaimer**

461 This study, to the best of the author(s) knowledge and belief, contains no material previously published or  
462 written by another person, except where due reference is made in the text of the study.

463

464 **Acknowledgements**

465 We acknowledge assistance from Simon Wotherspoon (Institute for Marine and Antarctic Studies) in  
466 appropriate model selection methods. We thank Lorraine Lisiecki and Constantijn Berends's for their  
467 constructive reviews, which greatly improved the manuscript. This research was supported by the Australian  
468 Government through Australian Antarctic Science projects 4632, the Million Year Ice Core (MYIC) Project and  
469 by the Australian Government Department of Industry Science Energy and Resources, grant ASCI000002.

470

471 **Data availability**

472 The model code and PRED-CO<sub>2</sub> data presented here is publicly archived at the Australian Antarctic Data Centre  
473 ([https://data.aad.gov.au/metadata/AAS\\_4632\\_Martin\\_etal\\_CP\\_2024](https://data.aad.gov.au/metadata/AAS_4632_Martin_etal_CP_2024))

474

475 **References**

- 476 Archer, D., Winguth, A., D. Lea, and Mahowald, N.: What caused the glacial/interglacial atmospheric  
477 pCO<sub>2</sub> cycle?, *Rev. Geophys.*, 38, 159–189, 2000, <https://doi.org/10.1029/1999RG000066>, 2000.
- 478  
479 Bazin, L., Landais, A., Lemieux-Dudon, B., Toye Mahamadou Kele, H., Veres, D., Parrenin, F., Martinerie, P.,  
480 Ritz, C., Capron, E., Lipenkov, V., Loutre, M.-F., Raynaud, D., Vinther, B., Svensson, A., Rasmussen, S.,  
481 Severi, M., Blunier, T., Leuenberger, M., Fischer, H., Masson-Delmotte, V., Chappellaz, J., and Wolff, E.: An  
482 optimized multi-proxies, multi-site Antarctic ice and gas orbital chronology (AICC2012): 120-800 ka, *Clim.*  
483 *Past*, 9, 1715-1731, <https://doi.org/10.5194/cp-9-1715-2013>, 2013.
- 484  
485 Bereiter, B., Eggleston, S., Schmitt, J., Nehrbass-Ahles, C., Stocker, T. F., Fischer, H., Kipfstuhl, S., and  
486 Chappellaz, J.: Revision of the EPICA Dome C CO<sub>2</sub> record from 800 to 600 ky before present, *Geophys. Res.*  
487 *Lett.*, 42, 542-549, <https://doi.org/10.1002/2014gl061957>, 2015.
- 488  
489 Berends, C. J., Köhler, P., Lourens, L. J., and van de Wal, R. S. W.: On the cause of the mid-Pleistocene  
490 transition., *Rev. Geophys.*, 59, e2020RG000727. <https://doi.org/10.1029/2020RG000727>, 2021a.
- 491  
492 Berends, C. J., de Boer, B., and van de Wal, R. S. W.: Reconstructing the evolution of ice sheets, sea level, and  
493 atmospheric CO<sub>2</sub> during the past 3.6 million years. *Clim. Past*, 17, 361–377, [http://doi.org/10.5194/cp-17-361-](http://doi.org/10.5194/cp-17-361-2021)  
494 [2021](http://doi.org/10.5194/cp-17-361-2021), 2021b.
- 495  
496 Berger, A., Li, X. S., and Loutre, M. F.: Modelling northern hemisphere ice volume over the last 3Ma,  
497 *Quaternary. Sci. Rev.*, 18, 1-11, [https://doi.org/10.1016/S0277-3791\(98\)00033-X](https://doi.org/10.1016/S0277-3791(98)00033-X), 1999.
- 498  
499 Broecker, W.S.: Glacial to interglacial changes in ocean chemistry, *Prog. Oceanogr.*, 11 (2), 151-197.  
500 [https://doi.org/10.1016/0079-6611\(82\)90007-6](https://doi.org/10.1016/0079-6611(82)90007-6), 1982.
- 501  
502 Chalk, T., Hain, M., Foster, G., Rohling, E., Sexton, P., Badger, M., Cherry, S., Hasenfratz, A., Haug, G.,  
503 Jaccard, S., Martínez-García, A., Pälike, H., Pancost, R., and Wilson, P.: Causes of ice age intensification across  
504 the Mid-Pleistocene Transition, *P. Natl. Acad. Sci. USA.*, 114, 13114-13119,  
505 <https://doi.org/10.1073/pnas.1702143114>, 2017.
- 506  
507 Clark, P. U., Archer, D., Pollard, D., Blum, J. D., Rial, J. A., Brovkin, V., Mix, A. C., Pisias, N. G., and Roy,  
508 M.: The middle Pleistocene transition: characteristics, mechanisms, and implications for long-term changes in  
509 atmospheric pCO<sub>2</sub>, *Quat. Sci. Rev.*, 25, 3150-3184, <https://doi.org/10.1016/j.quascirev.2006.07.008>, 2006.
- 510  
511 Clark, P. U. and Pollard, D.: Origin of the Middle Pleistocene Transition by ice sheet erosion of regolith,  
512 *Paleoceanography*, 13, 1-9, <https://doi.org/10.1029/97pa02660>, 1998.

513  
514 Dyez, K.A., Hönisch, B., and Schmidt, G.A.: Early Pleistocene obliquity-scale pCO<sub>2</sub> variability at ~1.5 million  
515 years ago. *Paleoceanogr. Paleoclimatol.*, 33, no. 11, 1270-1291, <https://doi.org/10.1029/2018PA003349>, 2018.  
516  
517 Elderfield, H., Ferretti, P., Greaves, S., Crowhurst, S., McCave, N., and Piotrowski, A.M.: Evolution of Ocean  
518 Temperature and Ice Volume Through the Mid-Pleistocene Climate Transition, *Science*, 337,704-709,  
519 <https://doi.org/10.1126/science.1221294>, 2012.  
520  
521 Gottschalk, J., Battaglia, G., Fischer, H., Frölicher, T.L., Jaccard, S.L., Jeltsch-Thömmes, A., Joos, F., Köhler,  
522 P., Meissner, K.J., Menviel, L., Nehrbass-Ahles, C., Schmitt, J., Schmittner, A., Skinner, L.C., and Stocker,  
523 T.G.: Mechanisms of millennial-scale atmospheric CO<sub>2</sub> change in numerical model simulations, *Quaternary*.  
524 *Sci. Rev.*, 220, 30-74, <https://doi.org/10.1016/j.quascirev.2019.05.013>, 2019.  
525  
526 Guillermic, M., Misra, S., Eagle, R., and Tripathi, A.: Atmospheric CO<sub>2</sub> estimates for the Miocene to Pleistocene  
527 based on foraminiferal δ<sup>11</sup>B at Ocean Drilling Program Sites 806 and 807 in the Western Equatorial Pacific,  
528 *Clim. Past*, 18(2), 183-207, <https://doi.org/10.5194/cp-18-183-2022>, 2022.  
529  
530 Hasenfratz, A. P., Jaccard, S. L., Martínez-García, A., Sigman, D. M., Hodell, D. A., Vance, D., Bernasconi, S.  
531 M., Kleiven, H. F., Haumann, F. A., and Haug, G. H.: The residence time of Southern Ocean surface waters and  
532 the 100,000-year ice age cycle, *Science*, 363, 1080, <https://doi.org/10.1126/science.aat7067>, 2019.  
533  
534 Higgins, J. A., Kurbatov, A. V., Spaulding, N. E., Brook, E., Introne, D. S., Chimiak, L. M., Yan, Y.,  
535 Mayewski, P. A., and Bender, M. L.: Atmospheric composition 1 million years ago from blue ice in the Allan  
536 Hills, Antarctica, *P. Natl. Acad. Sci. USA.*, 112, 6887, <https://doi.org/10.1073/pnas.1420232112>, 2015.  
537  
538 Hönisch, B., Hemming, N. G., Archer, D., Siddall, M., and McManus, J. F.: Atmospheric Carbon Dioxide  
539 Concentration Across the Mid-Pleistocene Transition, *Science*, 324, 1551,  
540 <https://doi.org/10.1126/science.1171477>, 2009.  
541  
542 Huybers, P., & Wunsch, C. (2005). Obliquity pacing of the late Pleistocene glacial terminations. *Nature*,  
543 434(7032), 491-494.  
544  
545 International Panel on Climate Change: Climate change 2001; IPCC third assessment report, IPCC, Geneva,  
546 2001.  
547  
548 International Partnerships in Ice Core Sciences: The oldest ice core: A 1.5 million year record of climate and  
549 greenhouse gases from Antarctica [White paper]. [https://igbp-](https://igbp-scor.pages.unibe.ch/sites/default/files/download/docs/working_groups/ipics/white-papers/ipics_oldda_final.pdf)  
550 [scor.pages.unibe.ch/sites/default/files/download/docs/working\\_groups/ipics/white-papers/ipics\\_oldda\\_final.pdf](https://igbp-scor.pages.unibe.ch/sites/default/files/download/docs/working_groups/ipics/white-papers/ipics_oldda_final.pdf),  
551 accessed 06/12/2023, 2020.  
552  
553 Jouzel, J., Masson-Delmotte, V., Cattani, O., Dreyfus, G., Falourd, S., Hoffmann, G., Minster, B., Nouet, J.,  
554 Barnola, J. M., Chappellaz, J., Fischer, H., Gallet, J. C., Johnsen, S., Leuenberger, M., Loulergue, L., Luethi, D.,  
555 Oerter, H., Parrenin, F., Raisbeck, G., Raynaud, D., Schilt, A., Schwander, J., Selmo, E., Souchez, R., Spahni,  
556 R., Stauffer, B., Steffensen, J. P., Stenni, B., Stocker, T. F., Tison, J. L., Werner, M., and Wolff, E. W.: Orbital  
557 and Millennial Antarctic Climate Variability over the Past 800,000 Years, *Science*, 317, 793,  
558 <https://doi.org/10.1126/science.1141038>, 2007.  
559  
560 Lisiecki, L. E. and Raymo, M. E.: A Pliocene-Pleistocene stack of 57 globally distributed benthic δ<sup>18</sup>O records,  
561 *Paleoceanography*, 20, PA1003, <https://doi.org/10.1029/2004pa001071>, 2005.  
562  
563 Martínez-García, A., Sigman, D.M., Ren, H., Anderson, R.F., Straub, M., Hodell, D.A., Jaccard, S.L., Eglinton,  
564 T.I., and Haug, G.H.: Iron fertilization of the subantarctic ocean during the last ice age, *Science*, 343 (6177),  
565 1347-1350, <https://doi.org/10.1126/science.1246848>, 2014.  
566  
567 McClymont, E.L., Sosdian, S.M., and Rosell-Melé, A.: Pleistocene sea-surface temperature evolution: Early  
568 cooling, delayed glacial intensification, and implications for the mid-Pleistocene transition. *Earth. Sci. Rev.*,  
569 123, 173-193, <https://doi.org/10.1016/j.earscirev.2013.04.006>, 2013.  
570  
571 Millero, F. J.: Thermodynamics of the carbon dioxide system in the oceans, *Geochim. Cosmochim. Acta.*, 59,  
572 661-677, [https://doi.org/10.1016/0016-7037\(94\)00354-O](https://doi.org/10.1016/0016-7037(94)00354-O), 1995.

573  
574 Morée, A. L., Sun, T., Bretones, A., Straume, E. O., Nisancioglu, K., and Gebbie, G.: Cancellation of the  
575 precessional cycle in  $\delta^{18}\text{O}$  records during the Early Pleistocene. *Geophys. Res. Lett.*, 48,  
576 e2020GL090035. <https://doi.org/10.1029/2020GL090035>, 2021.

577  
578 Petit, J. R., Jouzel, J., Raynaud, D., Barkov, N. I., Barnola, J. M., Basile, I., Bender, M., Chappellaz, J., Davis,  
579 M., Delaygue, G., Delmotte, M., Kotlyakov, V. M., Legrand, M., Lipenkov, V. Y., Lorius, C., Pépin, L., Ritz,  
580 C., Saltzman, E., and Stievenard, M.: Climate and atmospheric history of the past 420,000 years from the  
581 Vostok ice core, Antarctica, *Nature*, 399, 429-436, <https://doi.org/10.1038/20859>, 1999.

582  
583 Raymo, M., Lisiecki, L., and Nisancioglu, K.: Plio-Pleistocene Ice Volume, Antarctic Climate, and the Global  
584  $18\text{O}$  Record, *Science*, 313, 492-495, <https://doi.org/10.1126/science.1123296>, 2006.

585  
586 Raymo, M., Ruddiman, W., and Froelich, P.: Influence of Late Cenozoic mountain building on ocean  
587 geochemical cycles, *Geology*, 16, 649-653, [https://doi.org/10.1130/0091-](https://doi.org/10.1130/0091-7613(1988)016<0649:IOLCMB>2.3.CO;2)  
588 [7613\(1988\)016<0649:IOLCMB>2.3.CO;2](https://doi.org/10.1130/0091-7613(1988)016<0649:IOLCMB>2.3.CO;2), 1988.

589  
590 Raymo, M. E.: The timing of major climate terminations, *Paleoceanography*, 12, 577-585,  
591 <https://doi.org/10.1029/97PA01169>, 1997.

592  
593  
594 Röthlisberger, R., Bigler, M., Wolff, E. W., Joos, F., Monnin, E., and Hutterli, M. A.: Ice core evidence for the  
595 extent of past atmospheric  $\text{CO}_2$  change due to iron fertilisation, *Geophys. Res. Lett.*, 31, L16207,  
596 <https://doi.org/10.1029/2004GL020338>, 2004.

597  
598 Ruddiman, W. F., Raymo, M. E., Martinson, D. G., Clement, B. M., and Backman, J.: Pleistocene evolution:  
599 Northern hemisphere ice sheets and North Atlantic Ocean, *Paleoceanography*, 4, 353-412,  
600 <https://doi.org/10.1029/PA004i004p00353>, 1989.

601  
602 Shackleton, N. J. and Pisias, N. G.: Atmospheric Carbon Dioxide, Orbital Forcing, and Climate. In: *The Carbon*  
603 *Cycle and Atmospheric  $\text{CO}_2$ : Natural Variations Archean to Present*, <https://doi.org/10.1029/GM032p0303>,  
604 1985.

605  
606 Shugi, H., The older the ice, the better the science. *Adv. Polar Sci.*, 23, 121-122,  
607 <https://doi.org/10.13679/j.advps.2022.0004>, 2022.

608  
609 Stephens, B.B., Keeling, R.F.: The influence of Antarctic sea ice on glacial–interglacial  $\text{CO}_2$  variations. *Nature*,  
610 404, 171–174, <https://doi.org/10.1038/35004556>, 2000.

611  
612 Tzedakis, P. C., Crucifix, M., Mitsui, T., and Wolff, E. W.: A simple rule to determine which insolation cycles  
613 lead to interglacials, *Nature*, 542, 427-432, <https://doi.org/10.1038/nature21364>, 2017.

614  
615 Ushie, H., and Matsumoto, K.: The role of shelf nutrients on glacial-interglacial  $\text{CO}_2$ : A negative  
616 feedback, *Global Biogeochem. Cy.*, 26, GB2039, <https://doi.org/10.1029/2011GB004147>., 2012.

617  
618 van de Wal, R. S. W., de Boer, B., Lourens, L. J., Köhler, P., and Bintanja, R.: Reconstruction of a continuous  
619 high-resolution  $\text{CO}_2$  record over the past 20 million years. *Clim. Past*, 7, 1459–1469. [https://doi.org/10.5194/cp-](https://doi.org/10.5194/cp-7-1459-2011)  
620 [7-1459-2011](https://doi.org/10.5194/cp-7-1459-2011), 2011.

621  
622 Veres, D., Bazin, L., Landais, A., Toyé Mahamadou Kele, H., Lemieux-Dudon, B., Parrenin, F., Martinerie, P.,  
623 Blayo, E., Blunier, T., Capron, E., Chappellaz, J., Rasmussen, S., Severi, M., Svensson, A., Vinther, B., and  
624 Wolff, E.: The Antarctic ice core chronology (AICC2012): an optimized multi-parameter and multi-site dating  
625 approach for the last 120 thousand years, *Clim. Past*, 9, 1733-1748, <https://doi.org/10.5194/cp-9-1733-2013>,  
626 2013.

627  
628 Willeit, M., Ganopolski, A., Calov, R., and Brovkin, V.: Mid-Pleistocene transition in glacial cycles explained by  
629 declining  $\text{CO}_2$  and regolith removal, *Sci. Adv.*, 5, eaav7337, doi: 10.1126/sciadv.aav7337, 2019.

630



631 Wolff, E. W., Chappella, J., Fischer, H., Kull, C., Miller, H., Stocker, T. F., and Watson, A. J.: The EPICA  
632 challenge to the Earth system modeling community, *EOS*, 85, 363363, <https://doi.org/10.1029/2004EO380003>,  
633 2004.  
634  
635 Wolff, E. W., Kull, C., Chappellaz, J., Fischer, H., Miller, H., Stocker, T. F., Watson, A. J., Flower, B., Joos, F.,  
636 Köhler, P., Matsumoto, K., Monnin, E., Mudelsee, M., Paillard, D., and Shackleton, N.: Modeling past  
637 atmospheric CO<sub>2</sub>: results of a challenge, *EOS*, 86 (38), 341-345, <http://doi.org/10.1029/2005EO380003>, 2005.  
638  
639 Yamamoto, M., Clemens, S.C., Seki, O., Tsuchiya, Y., Huang, Y., O'ishi, R., and Abe-Ouchi, A.: Increased  
640 interglacial atmospheric CO<sub>2</sub> levels followed the mid-Pleistocene Transition, *Nat. Geosci.*, 15(4), 307–313,  
641 <https://doi.org/10.1038/s41561-022-00918-1>, 2022.  
642  
643 Yan, Y., Bender M.I., Brook, E.J., Clifford, H.M., Kemeny, P.C., Kurbatov, A.V., Mackay, S., Mayewski,  
644 P.A., Ng, J., Severinghaus J.P., and Higgins, J.A.: Two-million-year-old snapshots of atmospheric gases from  
645 Antarctic ice, *Nature*, 574(7780), 663–666, <https://doi.org/10.1038/s41586-019-1692-3>, 2019.  
646  
647 Yan, Y., Kurbatov, A.V., Mayewski, P.A., Shackleton, S., and Higgins, J.A.: Early Pleistocene East Antarctic  
648 temperature in phase with local insolation. *Nat. Geosci.*, 16, 50-55, [https://doi.org/10.1038/s41561-022-01095-](https://doi.org/10.1038/s41561-022-01095-x)  
649 x, 2022.